Cell Reports
Methods

Article

A genetic tool for the longitudinal study of a subset of post-inflammatory reactive astrocytes

Graphical abstract

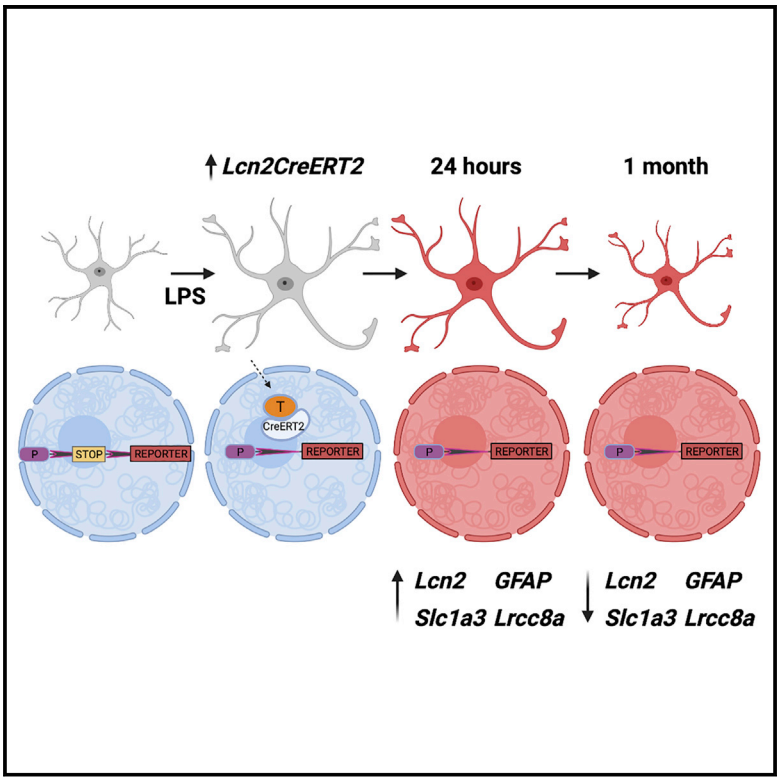

Highlights

- An inducible Cre line to selectively target a subset of reactive astrocytes (RAs)
- Cre is expressed in RAs across a wide array of brain inflammation models
- Enables the permanent tagging of RAs for longitudinal analysis
- RAs largely revert to a non-reactive state 1 month after acute inflammation

Authors

William Agnew-Svoboda, Teresa Ubina, Zoe Figueroa, ..., Emma H. Wilson, Todd A. Fiacco, Martin M. Riccomagno

Correspondence

toddf@ucr.edu (T.A.F.),
martinmr@ucr.edu (M.M.R.)

In brief

Agnew-Svoboda et al. generate an inducible Cre line to enable selective targeting and manipulation of a subset of reactive astrocytes (RAs) in brain disease. Longitudinal analysis of RAs reveal that astrocytes that become reactive soon after acute inflammation survive but largely revert to a non-reactive state once inflammation has resolved.

Agnew-Svoboda et al., 2022, Cell Reports Methods 2, 100276
August 22, 2022
https://doi.org/10.1016/j.crmeth.2022.100276

CellPress

Cell Reports Methods

CellPress
OPEN ACCESS

Article

A genetic tool for the longitudinal study of a subset of post-inflammatory reactive astrocytes

William Agnew-Svoboda,[1,2] Teresa Ubina,[1,2] Zoe Figueroa,[1,3] Yiu-Cheung Wong,[2,5] Edward A. Vizcarra,[3,4] Bryan Roebini,[2] Emma H. Wilson,[1,3,4] Todd A. Fiacco,[1,2,4,*] and Martin M. Riccomagno[1,2,4,6,*]

[1]Neuroscience Graduate Program, University of California, Riverside, Riverside, CA 92521, USA
[2]Department of Molecular, Cell, and Systems Biology, University of California, Riverside, Riverside, CA 92521, USA
[3]Division of Biomedical Sciences, University of California, Riverside, Riverside, CA 92521, USA
[4]Biomedical Sciences Graduate Program, University of California, Riverside, Riverside, CA 92521, USA
[5]Present address: Developmental Biology Program, Department of Developmental Biology, Stanford University, Stanford, CA 94305, USA
[6]Lead contact
*Correspondence: toddf@ucr.edu (T.A.F.), martinmr@ucr.edu (M.M.R.)
https://doi.org/10.1016/j.crmeth.2022.100276

MOTIVATION *In vivo* study of reactive astrocytes (RAs) has proven difficult mainly because existing genetic tools using traditional astrocyte promoters cannot distinguish between healthy versus reactive astrocytes. To fill this gap, we describe the generation and characterization of an inducible genetic tool that can be used to specifically target, label, and manipulate a subset of RAs in the diseased or injured brain. We provide evidence for the utility of this approach to study RAs in several models of brain inflammation.

SUMMARY

Astrocytes are vital support cells that ensure proper brain function. In brain disease, astrocytes reprogram into a reactive state that alters many of their cellular roles. A long-standing question in the field is whether downregulation of reactive astrocyte (RA) markers during resolution of inflammation is because these astrocytes revert back to a non-reactive state or die and are replaced. This has proven difficult to answer mainly because existing genetic tools cannot distinguish between healthy versus RAs. Here we describe the generation of an inducible genetic tool that can be used to specifically target and label a subset of RAs. Longitudinal analysis of an acute inflammation model using this tool revealed that the previously observed downregulation of RA markers after inflammation is likely due to changes in gene expression and not because of cell death. Our findings suggest that cellular changes associated with astrogliosis after acute inflammation are largely reversible.

INTRODUCTION

Astrocytes are the most abundant cell type in the CNS where they serve as critical regulators of homeostasis (Sofroniew and Vinters, 2010). In the healthy CNS, astrocytes provide synaptic support to neurons, facilitate transport of nutrients and waste, and maintain the blood-brain barrier (BBB) (Engelhardt and Sorokin, 2009; Jessen et al., 2015; Panatier and Robitaille, 2016). The BBB isolates the CNS from the circulating immune system of the periphery, so the brain has evolved its own innate immune system where local glia are immune responders (Escartin et al., 2021). This process is known as reactive gliosis, where microglia and astrocytes become reactive following inflammation. Reactive astrocytes (RAs) occur in any CNS inflammatory response, and have been observed after a variety of insults such as penetrating brain injuries, epilepsy, and Alzheimer disease (Binder and Steinhauser, 2006; Burda and Sofroniew, 2014; Katsouri et al., 2020; Laird et al., 2008). Reactivity in astrocytes has historically been identified by the hypertrophy of its major processes and upregulation of the intermediate filament glial fibrillary acidic protein (GFAP) (Anderson et al., 2014; Eng et al., 1971). In response to severe damage, astrocytes can migrate and polarize to form a glial scar, or even reenter the cell cycle and proliferate (Ferrer-Acosta et al., 2017; Wanner et al., 2013).

Despite the prevalence of this response, many questions remain regarding the function of RAs. Some evidence suggests that reactivity in astrocytes is harmful to CNS repair and recovery, whereas more recent data suggest that preventing reactivity actually increases the damage caused by a brain injury (Katsouri et al., 2020; Liddelow et al., 2017; Okada et al., 2006; Shinozaki et al., 2017; Yun et al., 2018). Little is known about the differences in reactive responses across different disease models,

with studies suggesting that there may be great variability in astrocyte gene expression in a disease-dependent manner (Park et al., 2021; Yun et al., 2018; Zamanian et al., 2012). Furthermore, within a given disease, astrocyte reactivity may vary both regionally and temporally, with some astrocytes remaining completely unreactive (Sofroniew, 2020; Wheeler et al., 2020; Zamanian et al., 2012).

These outstanding questions can begin to be addressed through development of new tools to specifically target RAs and observe their behavior, physiology, and gene expression over time. Existing tools used to study RAs have the limitation of also being expressed in healthy astrocytes, and are not able to target RAs at specific time points in the inflammatory response or in the progression of disease (Cahoy et al., 2008; Robel et al., 2009; Sofroniew, 2009). The recent identification of genes that are upregulated only in RAs has provided a means to begin to address these limitations. *Lipocalin-2* (*Lcn2*), an iron chelator expressed abundantly in the peripheral immune system but at negligible levels in the healthy brain, was identified as being upregulated strongly in RAs in mouse models of inflammation and stroke (Zamanian et al., 2012). Initially deemed a pan-RA marker, *Lcn2* has more recently been shown to be upregulated to varying degrees in a large pool of astrocytes in several disease models, with some exceptions (Diaz-Castro et al., 2019; Habib et al., 2020; Hasel et al., 2021; Liddelow et al., 2017; Zamanian et al., 2012). Based on this knowledge, we developed a *Lcn2CreERT2* mouse that expresses a tamoxifen-dependent Cre recombinase (Cre-ERT2) under the *Lcn2* promoter.

Using the *Lcn2CreERT2* mouse, we were able to examine RAs across a variety of brain inflammation models and isolate labeled cells to be used for single cell studies. This transgenic tool can be used to permanently label RAs soon after a brain insult and follow them over time. This allows for longitudinal studies of RA morphology, physiology, and gene expression after the onset of a particular neuropathology. Using this approach, we demonstrate that astrocytes labeled in response to an acute inflammatory insult remain in the CNS after inflammation is resolved, while expression of traditional reactive markers returns to a baseline level. Overall, our experiments suggest that most RAs remain alive after the resolution of inflammation. Interestingly, while gene expression and morphology appear to largely revert back to baseline levels, some morphological features of reactivity might remain a month after inflammation. Our data highlight the potential of the *Lcn2CreERT2* mouse to advance understanding of astrocyte reactivity and identify new underlying disease mechanisms.

RESULTS

Validation of Lcn2 as a RA marker and design of the Lcn2CreERT2 mouse

Lcn2 expression has been previously shown to be upregulated hundreds of fold in mouse models of stroke and systemic inflammation (Liddelow et al., 2017; Zamanian et al., 2012). To confirm that *Lcn2* is strongly upregulated in astrocytes following an inflammatory insult, Swiss Webster mice were injected with 5 mg/kg lipopolysaccharide (LPS) or equivalent saline intraperitoneally (IP) and collected after 24 h. Forebrains were analyzed for expression of *Lcn2* along with the astrocyte marker *SLC1a3* (GLAST/EAAT1) by means of fluorescence *in situ* hybridization (FISH) using RNAScope (Figure S1A). While *Lcn2* expression in saline-treated brains was not detected, it was upregulated in LPS-treated mice over 266-fold, consistent with previous studies (Zamanian et al., 2012) (Figure S1A). The aforementioned study that identified *Lcn2* upregulation in RAs also described some expression in endothelial cells (Zamanian et al., 2012). Therefore, cells were co-stained for the endothelial cell marker platelet and endothelial cell adhesion molecule 1 (*PECAM1*). Lcn2 also co-localized with PECAM1 by FISH (Figure S1A). As expected from previous studies, our results indicated negligible *Lcn2* expression in control brain tissue with several fold increase 1 day after an acute inflammatory insult, with expression observed in astrocytes (*SLC1a3*+) and endothelial cells (*PECAM1*+).

After validating strong upregulation of *Lcn2* only in LPS-treated animals, we decided to target the *Lcn2* locus by homologous recombination to develop an *Lcn2CreERT2* mouse. To generate this mouse, a *CreERT2* transgene followed by a P2A signal was targeted downstream of the endogenous *Lcn2* promoter and start codon, but upstream of the rest of the first coding exon (Figure S1B). Under this design, it was expected that the transgene would drive expression of a tamoxifen-inducible Cre in cells where *Lcn2* is expressed, without affecting endogenous *Lcn2* expression.

Validation of the Lcn2CreERT2 mouse during systemic inflammation

To begin to characterize this newly developed mouse line, the *Lcn2CreERT2* mouse was crossed into the Cre-reporter line *Ai9* (Madisen et al., 2010). This cross generates mice that express the red fluorescent tdTomato reporter in a Cre-dependent manner. Using the progeny from this cross, we tested the expression of *Lcn2CreERT2* following a 5-day low-dose LPS treatment protocol (Nava Catorce and Gevorkian, 2016). To ensure that expression was dependent on treatment with both LPS and tamoxifen, control animals were given saline and tamoxifen, saline and oil, or LPS and oil. Following the last day of treatment, brains were collected and immunohistochemistry was performed for the expression of tdTomato. This revealed that tdTomato was strongly upregulated in animals treated with both LPS and tamoxifen; however, its expression was negligible in all other treatment groups (Figures 1A and 1B). These results suggest that *Lcn2CreERT2*-dependent recombination occurs in an inflammation- and tamoxifen-dependent manner. The most robust expression of the Cre-dependent reporter was observed in the thalamus. Therefore, subsequent experiments focused on this region.

Next, we wanted to explore which cell types were expressing the Cre-dependent reporter. *Lcn2CreERT2*;*Ai9* brains from animals that received LPS and tamoxifen were stained for the neuronal marker NeuN, the astrocyte marker GFAP, the microglia marker Iba1, and the endothelial/microglial marker tomato lectin (Figures 1C and 1D). No tdTomato-expressing cells were found to be NeuN positive, whereas 51% ± 2.2% of tdTomato$^+$ cells were co-positive for lectin and 45% ± 1.8% of tdTomato$^+$ cells were co-positive for GFAP. The morphology of the

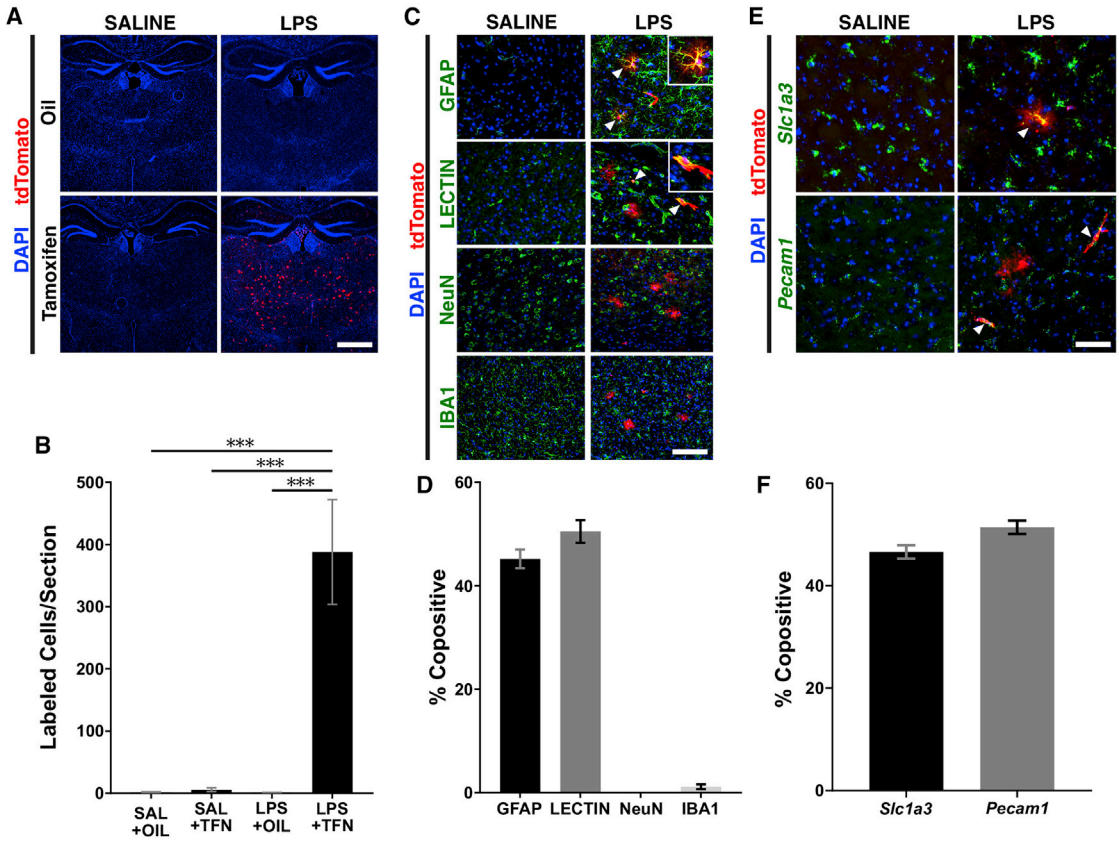

Figure 1. Expression of *Lcn2CreERT2* following repeated low-dose LPS treatment

(A) Immunostaining for tdTomato in *Lcn2CreERT2*;*Ai9* brains. Animals were given one of the following four treatments for 5 consecutive days: Saline and corn oil, saline and tamoxifen, LPS and corn oil, LPS and tamoxifen. Sections were counterstained with DAPI.

(B) Quantification of total number of red cells/section from animals in (A). ***$p < 0.001$ ANOVA and Tukey's post hoc test, n = 5 animals per treatment.

(C) Immunostaining of brains from saline- (left) or LPS-treated (right) *Lcn2CreERT2*;*Ai9* animals for tdTomato and the astrocytic marker GFAP (top), the endothelial and microglial marker lectin (second row), the neuronal marker NeuN (third row), and the microglial marker Iba1 (bottom). Sections were counterstained with DAPI. White arrowheads indicate co-positive cells for tdTomato and the panel maker.

(D) Quantification of co-positive cells from (C).

(E) RNAscope for the astrocytic marker *Slc1a3* (top) and the endothelial marker *Pecam1* (bottom) on brains from LPS- and saline-treated *Lcn2CreERT2*;*Ai9* animals. Sections were immunostained for tdTomato and counterstained with DAPI.

(F) Quantification of cells co-positive for tdTomato and RNA markers described in (E). Scale bars, (A) 250 μm, (C) 50 μm, (E) 25 μm. Error bars ± SEM.

See also Figures S1 and S2.

lectin-positive cells suggested that they were most likely endothelial cells, whereas the GFAP-positive cells appeared to be astrocytes; 20.31% ± 2.60% of the GFAP$^+$ astrocytes in the thalamus were colabeled with tdTomato. Only a small subset of tdTomato$^+$ cells was co-positive for Iba1 (1.1% ± 0.4%). Similar induction was observed after a single high dose of LPS, but the low-dose LPS protocol produced more consistent results (Figures S2A–S2E; n = 20 high-dose LPS animals). Thus, we adopted this low-dose protocol as the acute inflammatory treatment for the remainder of the study.

To further confirm the identity of the great majority of tdTomato-positive cells, we performed RNAScope staining for astrocytic *Slc1a3* and endothelial *Pecam1* in the brains of the LPS- and tamoxifen-treated *Lcn2CreERT2*;*Ai9* mice (Figures 1E and 1F). Using this technique, 47% ± 1.3% of identified tdTomato$^+$ cells were shown to be co-positive for *Slc1a3*, whereas 51% ± 1.3% were co-positive for *Pecam1*, consistent with the immunostaining results. Taken together, these data suggest that *Lcn2CreERT2* is expressed in the CNS only after an inflammatory insult and only when tamoxifen is present, and that its expression is found primarily in RAs and endothelial cells.

Expression of Lcn2CreERT2 in other brain injury models

We next examined whether the *Lcn2CreERT2* mouse could serve as a tool for the study of RAs across a range of disease and brain injury models. While several models were briefly explored for proof-of-concept (Figures S3A–S3C), here we highlight two in particular: Parasitic infection by *Toxoplasma gondii*, and direct CNS exposure to LPS through striatal LPS injections (Figures 2 and 3). In order to test whether *Lcn2CreERT2* mice will be useful for study of brain infection, *Lcn2CreERT2*;*Ai9* mice were infected with 20 *T. gondii* cysts IP or given a sham

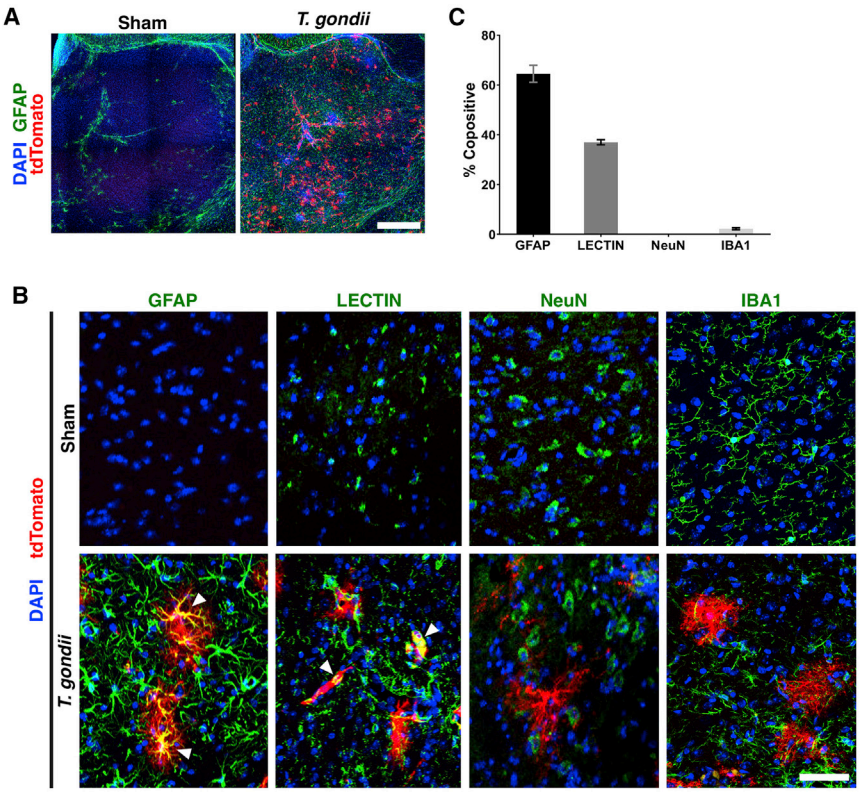

Figure 2. Expression of Lcn2CreERT2 in a parasitic model of neuroinflammation

(A) Immunostaining for tdTomato on *Lcn2CreERT2*; *Ai9* thalami 7 weeks after infection with *T. gondii*.

(B and C) Tissue from animals described in (A) was immunostained for tdTomato and the astrocytic marker GFAP (left), the endothelial and microglial marker lectin (second column), the neuronal marker NeuN, and the microglial marker Iba1(right). Co-positive cells indicated by white arrowheads, quantified in (C). n = 3 animals. Scale bars, (A) 250 μm, (B) 50 μm. Error bars ± SEM.

See also Figure S3.

injection of saline (Noor et al., 2010). *T. gondii* infection is a common human pathogen that exists in approximately one-third of the world's population and can cause serious life-threatening disease in the immune-compromised (Dubey et al., 2021). The parasite resides as cysts within neurons, requiring a continuous immune response in the brain to prevent reactivation and disease (Wohlfert et al., 2017). It therefore provides a model of chronic inflammation that is human disease-relevant. Three weeks following infection with *T. gondii*, animals were given tamoxifen three times a week for 4 weeks and collected after the last treatment. Expression of tdTomato was restricted to infected animals, while remaining below detection levels in sham controls (Figure 2A). The identity of the cells that turned on the reporter was investigated by co-labeling with neuronal, astrocytic, microglial, and endothelial markers. Of the tdTomato$^+$ cells, zero were found to be NeuN positive, 64% ± 3.4% were colabeled with GFAP, 37% ± 1% were colabeled for tomato lectin, and 2.3% ± 0.4% were positive for Iba-1 (Figures 2B and 2C). Of the total number of GFAP$^+$ astrocytes in the thalamus, 18.36% ± 0.55% were also positive for tdTomato. These data suggest robust upregulation of *Lcn2CreERT2* following long-term *T. gondii* infection that was confined to astrocytes (predominantly) and endothelial cells as expected. Importantly, our data also revealed that *Lcn2CreERT2* is not induced by long-term treatment with tamoxifen alone.

We also looked at directly exposing the CNS to LPS via striatal injection, a model adapted from Hunter et al., who showed that striatal LPS injections could induce dramatic inflammation, followed by dopaminergic neuronal loss in the substantia nigra (Hunter et al., 2009). We reasoned that this could also serve as a relevant model of encephalitis. Expression of tdTomato could be found broadly and abundantly in the brain of LPS injected animals, whereas expression was much lower and restricted to the injection site in the saline-injected animals (Figures 3A and 3B). As observed in the other inflammation models, tdTomato was almost exclusively expressed by astrocytes and endothelial cells (Figures 3C and 3D). Taken together, our results suggest that many conditions that induce an inflammatory immune response in the brain will result in *Lcn2* expression, highlighting the utility of the *Lcn2CreERT2* mouse for the study of reactivity across multiple disease and brain injury models.

Flow sorting of labeled cells using the Lcn2CreERT2 mouse

The ability of the *Lcn2CreERT2* mouse to label reactive cells with a fluorescent marker opens the door to fluorescent-activated cell sorting (FACS) through flow cytometry, which enables the isolation and characterization of permanently labeled cells. As proof-of-concept, *Lcn2CreERT2*;*Ai9* animals underwent low-dose LPS treatment for 5 consecutive days, as described above. Twenty-four hours after the final LPS treatment, animals were killed and their brains prepared as a single cell suspension using needle passage and enzymatic digestion as described in the methods. Isolated cells were incubated with DAPI in order to identify dead cells, and sorted based on DAPI-negative, tdTomato-positive gates. As a percentage of live cells, tdTomato-expressing cells represented ~1.5% to 3% of the total cell population (Figure S4A). These results demonstrate the utility of the *Lcn2CreERT2* mouse for profiling and sequencing studies of a subset of RAs through their isolation by fluorescence cell sorting.

Combinatorial approaches using the Lcn2CreERT2 mouse to isolate specific reactive cell types

While *Lcn2CreERT2* expression appears only after an immune challenge, immunohistochemistry (IHC) and RNAScope revealed other "reactive" cell types in addition to astrocytes, namely endothelial cells and a very small percentage of

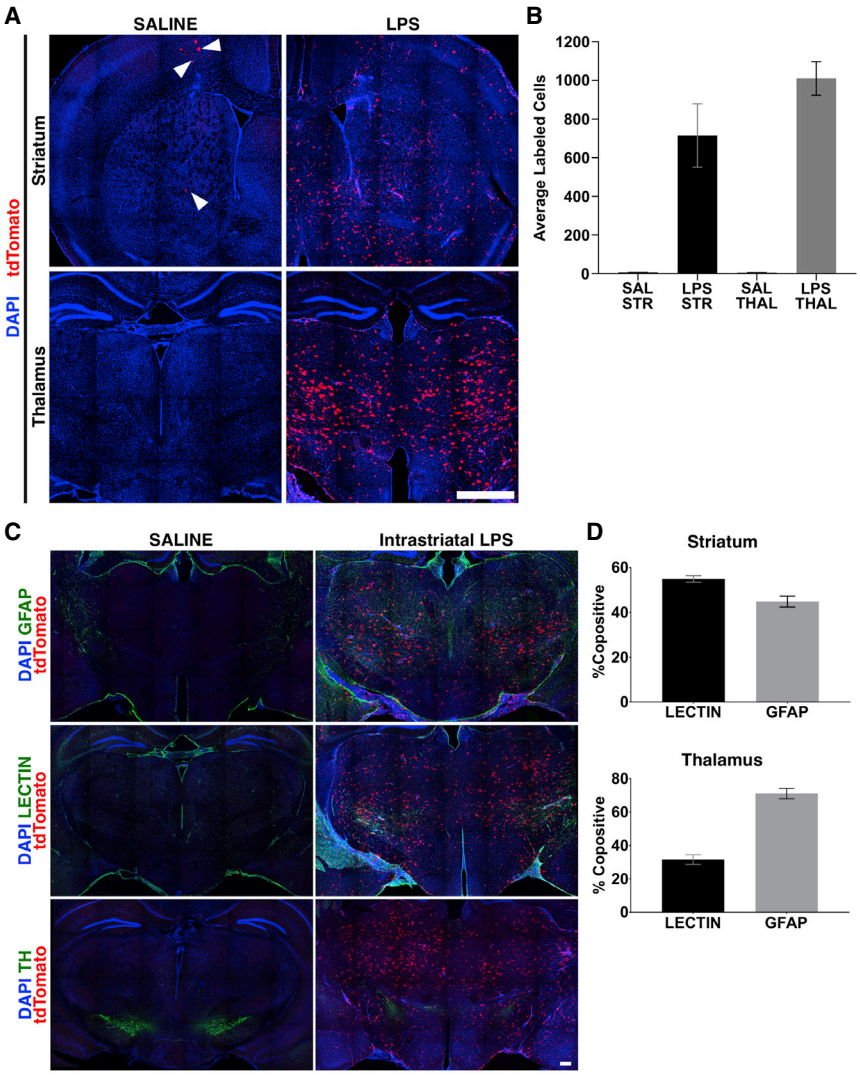

Figure 3. *Lcn2CreERT2;Ai9* tdTomato labeling after intrastriatal LPS injections

(A) tdTomato immunostaining of *Lcn2CreERT2;Ai9* animals injected intrastriatally with LPS or sterile saline and gavaged with tamoxifen for 3 days. Sections were counterstained with DAPI. tdTomato$^+$ cells lining the saline injection site are marked by white arrowheads.

(B) Quantification of total number of labeled cells in the striatum and thalamic regions.

(C) Representative images of brains collected after saline or LPS injections into the striatum (n = 4 animals). Coronal sections through the thalamus and ventral tegmental area were immunolabeled with anti-TdTomato antibody (red) and co-stained with DAPI (blue) and anti-GFAP (top, green), Lectin (middle, green) or tyrosine hydroxylase (bottom, TH, green). TdTomato signal partially co-localized with GFAP and lectin, but not with TH-positive catecholaminergic neurons.

(D) Quantification of cells co-positive for tdTomato and GFAP or lectin. Scale bars, (A) 250 μm, (C) 500 μm. Error bars ± SEM.

See also Figure S3.

microglial cells that were also Cre positive. In order to specifically drive expression in RAs, we designed an adeno-associated virus (AAV) to express a gene of interest (GOI) under the *Gfap* 2.2 promoter in a Cre-dependent manner (Figures S4B and S4C) (Atasoy et al., 2008; Lee et al., 2008; Schnütgen et al., 2003). A similar approach using the $Gfap_{ABC}$ promoter has been successfully implemented to study healthy astrocytes (Ung et al., 2020). There are several benefits to this combinatorial approach. First, use of a long *Gfap* promoter to drive GOIs in a Lcn2Cre-dependent manner ensures expression only in cells that are astrocytes (GFAP$^+$) and are reactive (*Lcn2CreERT2*$^+$). Second, targeting of specific brain regions can be achieved by injecting the newly designed AAVs stereotactically (Cetin et al., 2006). Broader expression of the GOI can be obtained by performing intraventricular injections in neonatal pups (Passini et al., 2003; Stoica et al., 2013).

To validate this approach, *Lcn2CreERT2* animals were injected into the right thalamus with AAV-*GFAP(long)-FLEX-GCaMP7f*, which drives expression of the calcium indicator GCaMP7f (Helassa et al., 2016) only in cells expressing GFAP and Cre together. Three weeks following injection of the virus, animals were treated with tamoxifen and LPS or saline as described in the methods section. Although there was some local signal in both saline- and LPS-treated animals around the viral injection site, expression in LPS-treated animals was much stronger and broader, confirming that acute inflammation induced expression of the reporter in RAs (Figures S4D and S4E). This result suggests that the combinatorial approach will be a powerful and adaptable method for using the *Lcn2CreERT2* mice to study reactive astrogliosis and in principle, other cell types activated in response to injury.

Lcn2Cre-expressing astrocytes remain in the CNS following resolution of inflammation

The fate of RAs after inflammation is resolved has been a fundamental question in the field (Escartin et al., 2021; Zamanian et al., 2012). Markers of RAs are rapidly induced after LPS treatment, but return to basal levels within 1 month (Escartin et al., 2021; Zamanian et al., 2012). Whether this overall decrease in expression of RA markers is a result of programmed cell death and generation of new cells, or downregulation of expression of these genes within RAs cannot be determined without an approach that permanently labels astrocytes at the onset of gliosis. In order to address this, low-dose LPS treatment was performed on *Lcn2CreERT2;Ai9* animals. Lcn2Cre-expressing cells were activated during the initial stages of inflammation by tamoxifen gavage, and brains collected at two separate time points for analysis by IHC: 24 h and 1 month after the final LPS treatment

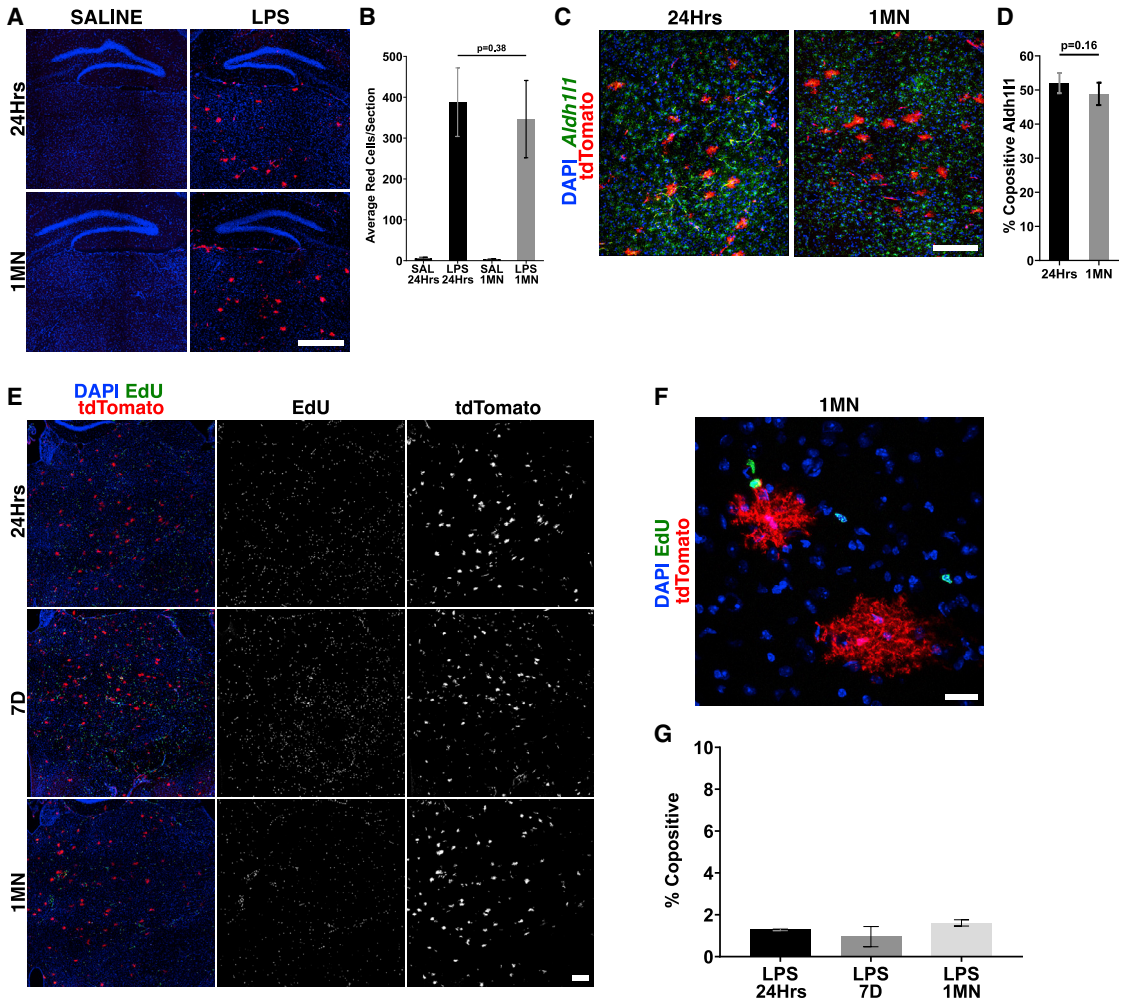

Figure 4. Astrocytes that were initially reactive remain in the brain after resolution of inflammation

(A) *Lcn2CreERT2;Ai9* brain sections immunostained for tdTomato and counterstained with DAPI. Animals were given tamoxifen and saline or LPS and collected at either 24 h or 1 month after the last treatment.

(B) Quantification of tdTomato-positive cells in the thalamic region. p = 0.38, ANOVA followed by Tukey's HSD post hoc, n = 5 animals.

(C) RNAScope on *Lcn2CreERT2;Ai9* brain sections for the astrocyte marker *Aldh1l1* 24 h and 1 month after low-dose LPS treatment, followed by immunostaining for tdTomato and counterstaining with DAPI.

(D) Quantification of *Aldh1l1* and tdTomato co-positive cells in (C). p = 0.16, paired t test. n = 18 pooled sections across three animals.

(E) Co-labeling of tdTomato and EdU-positive astrocytes in *Lcn2CreERT2;Ai9* animals after LPS treatment.

(F) High magnification image of labeled astrocytes and EdU-positive cells at 1 month.

(G) Quantification of tdTomato and EdU co-positive astrocytes at 24 h, 7 days, and 1 month following LPS treatment. Error bars ± SEM. Scale bars, (A) 400 μm, (C, E) 200 μm, (F) 20 μm.

See also Figure S4.

when reactive marker expression in the forebrain has returned to basal levels (Zamanian et al., 2012). While tdTomato signal remained negligible in saline-treated animals, it was robustly expressed in animals collected at both 24 h and 1 month (Figures 4A and 4B). The percentage of tdTomato$^+$ cells at 1 month was not significantly different compared with the proportion observed at 24 h (Figure 4B, *t(4)*=0.32, p = 0.38). Moreover, analysis of RNAScope data revealed no significant difference in the number of tdTomato$^+$ cells that expressed the astrocytic marker *ALDH1L1* at the two time points (Figures 4C and 4D; t = −1.000726, p = 0.160803). These results suggest that astrocytes that had become reactive and expressed *Lcn2CreERT2* at the onset of inflammation remain in the CNS long after inflammation has resolved.

To confirm that the numbers of tdTomato$^+$ astrocytes were not maintained via clonal expansion of just a few *Lcn2*$^+$ RAs that remained alive soon after the inflammatory insult subsided, we labeled proliferating cells at the peak of inflammation with Ethynyl deoxyUridine (EdU; Figures 4E–4G). EdU is a thymidine analog that is incorporated in cells undergoing the S-phase of

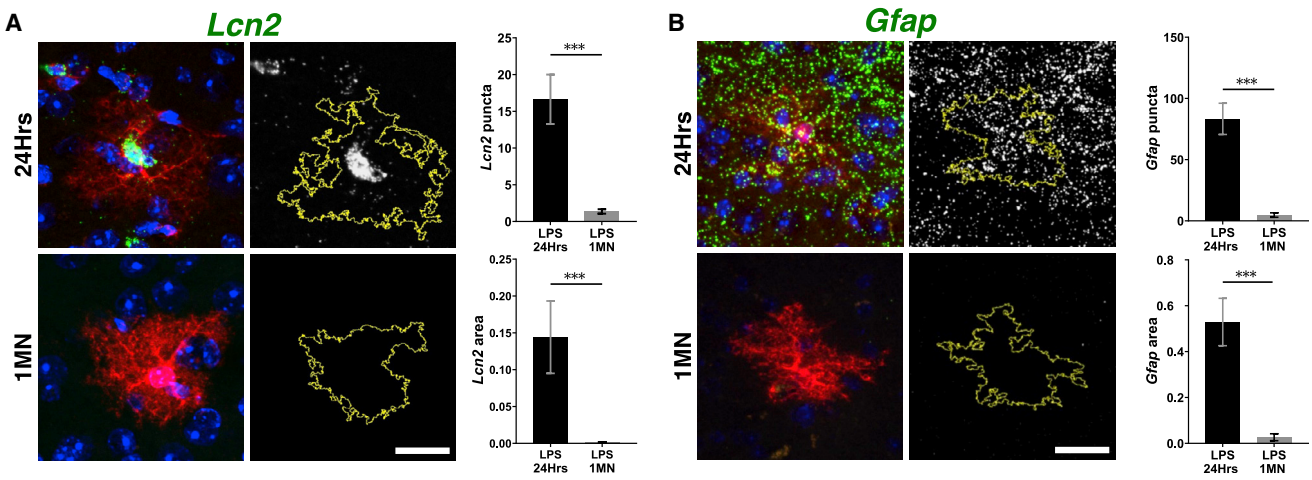

Figure 5. Reactive marker expression decreases 1 month after inflammation

(A and B) Analysis of reactive marker expression within tdTomato-positive cells. RNAScope for brain sections 24 h after LPS, or 1 month after LPS treatment to detect expression of the reactive markers *Lcn2* (A) and *GFAP* (B), followed by immunostaining for tdTomato and counterstaining with DAPI. RNAScope for reactive markers *Lcn2* (A) and *GFAP* (B) was quantified by looking at both number of fluorescent puncta (A, B, top panels) and integrated fluorescent density (A, B, bottom panels). ***$p < 0.001$, paired t test. n = 29 astrocytes pooled from three animals. Error bars ± SEM. Scale bars, 50 μm.
See also Figure S5.

the cell cycle (Salic and Mitchison, 2008) and can be used to observe the fate of cells born at a specific timepoint. EdU was injected on the last 2 days of the low-dose LPS treatment and also 22 h after. Brains were collected 24 h, 7 days, and 1 month after the low-dose treatment. Only a small percentage of tdTomato astrocytes appeared to be proliferative when collected at 24 h post -LPS. This tdTomato$^+$/EdU$^+$ population did not expand significantly, as the percentage remained almost constant at 7 days and 1 month after LPS (Figures 4E–4G; NS; one-way ANOVA). These data suggest that acute inflammatory insult does not result in noteworthy proliferation of RAs, and provides further support to the idea that the large majority of *Lcn2*$^+$ RAs remain alive 1 month after inflammation.

Morphological and molecular changes in RAs following inflammation

Next, we wanted to investigate whether the tdTomato-expressing cells maintained their expression of reactive markers, or if these returned to basal levels. We performed RNAScope on low-dose LPS- and saline-treated control animals collected at 24 h and 1 month after the final treatment, looking at overall expression of *GFAP* and *Lcn2* mRNA (Figures S5A and S5B). In support of the findings made by Zamanian et al. (2012), *Lcn2* was upregulated in animals collected 24 h after LPS treatment when compared with saline-treated animals and animals collected 1 month post LPS (Figures S5A and S5B; p = 0.00000 and p = 0.00000, respectively); 32.79% ± 4.68% of *Lcn2*$^+$ cells in the thalamus expressed tdTomato 24 h after LPS. Furthermore, there was no significant difference in *Lcn2* expression between animals treated with saline, and animals treated with LPS collected 1 month after treatment (Figure S5B; p = 0.99989). Similarly, *GFAP* was significantly upregulated in LPS-treated animals collected at 24 h relative to other groups (p = 0.00145, p = 0.00293), with no difference between saline control animals and animals collected 1 month after LPS (Figure S5B; p = 0.96454). These results confirm that the upregulated reactive markers *Lcn2* and *GFAP* return to much lower levels of expression once acute inflammation has resolved.

Together, the sustained levels of tdTomato signal with the longitudinal changes in reactive markers between early versus late time points suggest that RAs can revert to the non-reactive state after acute inflammation subsides. To confirm this, we identified astrocytes in LPS-treated animals collected at both 24 h and 1 month that were expressing tdTomato, indicating that they had at one point upregulated *Lcn2*. Expression of *Lcn2* and *GFAP* in these cells was examined by RNAScope in animals collected at both time points (Figures 5A and 5B). *Lcn2* fluorescence was much higher in cells from animals collected at the 24-h time point compared with 1 month (Figure 5A; $t(29) = 2.90272$, p = 0.002612). Similarly, *GFAP* was also upregulated in tdTomato-positive cells collected at 24 h relative to those at 1 month (Figure 5B, $t(29) = 4.91487$, $p < 0.00001$). These results suggest that these two reactive markers are only transiently upregulated in astrocytes following inflammation.

Based on this initial result, we probed deeper into the changes that astrocytes undergo after the resolution of inflammation by assessing independent measures of reactivity, i.e., alterations in volume and branching pattern (Escartin et al., 2021; Wilhelmsson et al., 2006). The use of a cytoplasmic tdTomato reporter has the advantage of allowing the visualization of the whole astrocyte and not just GFAP or other cytoskeletal features, thus providing a strong readout for morphological changes in thin astrocytic processes (Escartin et al., 2021). We compared the volume and branching pattern of tdTomato$^+$ astrocytes in *Aldh1l1CreERT2*;*Ai9* animals treated with saline and tamoxifen, versus astrocytes in *Lcn2CreERT2*;*Ai9* mice 24 h and 1 month after low-dose LPS treatment (Figures 6A and 6B). Consistent with previous studies (Wilhelmsson et al., 2006), cell volume did not

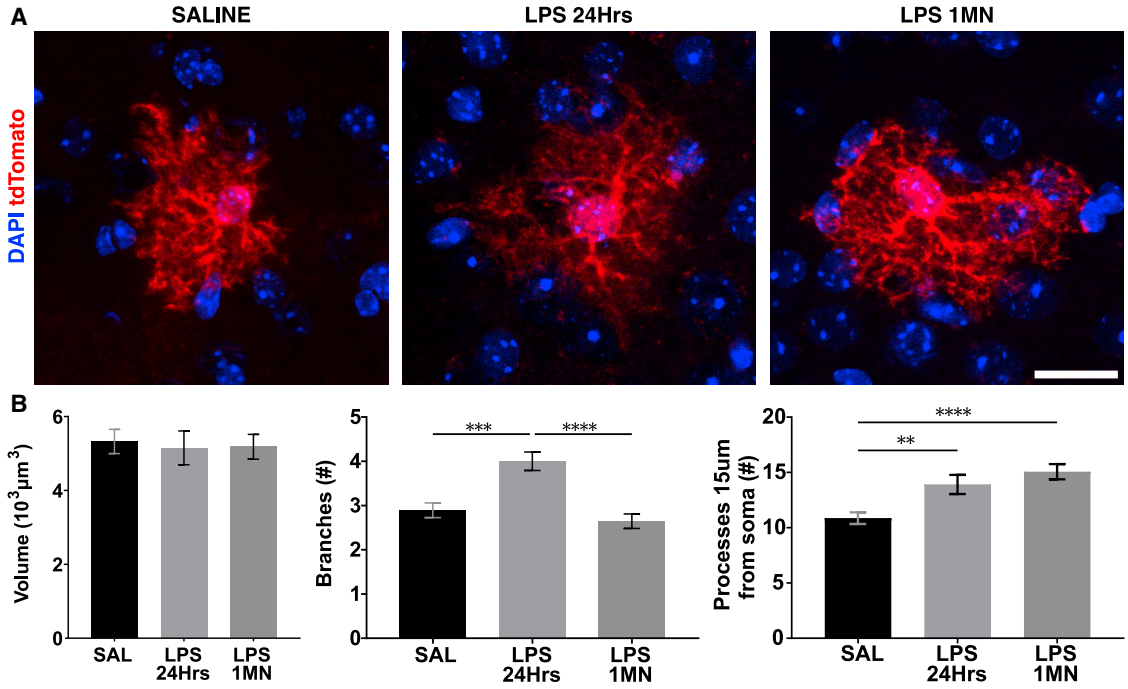

Figure 6. Morphological changes in astrocytes pre and post inflammation

(A) Representative morphology of tdTomato-positive astrocytes in *Lcn2CreERT2;Ai9* animals treated with saline or LPS, collected at 24 h and 1 month after treatment (top).

(B) Quantification of volume (bottom left), number of primary branches (bottom, middle), and number of processes 15 μm from the soma (bottom, right). $^{**}p < 0.01$, $^{***}p < 0.001$, $^{****}p < 0.0001$, ANOVA followed by Tukey's honest significant difference post hoc test. n = 30 pooled astrocytes across three animals. Error bars ± SEM. Scale bar, 20 μm.

significantly change after insult (Figures 6A and 6B; NS, one-way ANOVA). The number of total branches and the number of distal processes were significantly higher 24 h after LPS treatment versus saline treatment (Figure 6B; p = 0.0002 and p = 0.0068, respectively, one-way ANOVA followed by Tukey post hoc test). Interestingly, while the overall number of branches returned to baseline 1 month after LPS treatment, the number of distal processes did not (Figures 6A and 6B; saline versus 1 month, NS and p < 0.0001, respectively). This demonstrated that while some traditional markers of reactivity revert back to the non-reactive baseline, there are some longer-lasting effects of acute inflammation on astrocyte morphology.

To gain a better understanding of the resolution process in astrocytes, we visualized the expression of three physiologically relevant astrocyte-expressed genes at different timepoints after inflammation using RNAScope (Figures 7A–7C). Two glutamate transporters (*Slc1a3* and *Slc1a2*) and the pore-forming subunit of the Volume-Regulated Anion Channel (VRAC, *Lrrc8a*) that are known to be misregulated in a variety of brain disease models were chosen for this assessment (Diaz-Castro et al., 2019; Hasel et al., 2021; Peterson and Binder, 2019; Yang et al., 2019). Saline-injected, tamoxifen-induced *Aldh1l1-CreERT2*; *Ai9* animals were used to measure baseline expression. *Slc1a2* (GLT-1/EAAT2) expression in tdTomato$^+$ astrocytes did not significantly change after LPS treatment compared with saline-injected mice (Figure 7A; NS, one-way ANOVA). On the other hand, *Slc1a3* expression increased significantly 24 h after LPS treatment, but reverted back to baseline within 7 days (Figure 7B; p = 0.022 saline versus 24 h, p = 0.99 saline versus 7D, p = 0.61 saline versus 1 month). *Lrrc8a* showed a similar temporal pattern of expression as *Slc1a3*, increasing significantly in tdTomato$^+$ astrocytes 24 h after LPS treatment, but decreasing to the same level as saline-injected animals 7 days after LPS (Figure 7C; p = 0.0004 saline versus 24 h, p = 0.3 saline versus 7D, p = 0.75 saline versus 1 month). Taken together, our findings suggest that astrocytes that upregulate reactive markers following inflammation survive in the brain while no longer strongly expressing some of these markers after inflammation has resolved.

DISCUSSION

Reactive gliosis is an early response to brain inflammation, which occurs universally in brain pathologies including infection, trauma, and neurodegenerative disease (Sofroniew, 2020). While astrocyte reactivity has been observed in many contexts, very little remains known about how RAs participate in positive or negative outcomes (Escartin et al., 2021). An astrocyte reacting to a beta amyloid plaque in Alzheimer disease may upregulate GFAP in the same way it does in response to a penetrating brain injury, but questions remain about how similar these responses really are. Such questions can only be answered by examining reactivity in a context-dependent manner in great detail. In order to do so, new tools are needed that allow RAs to be targeted

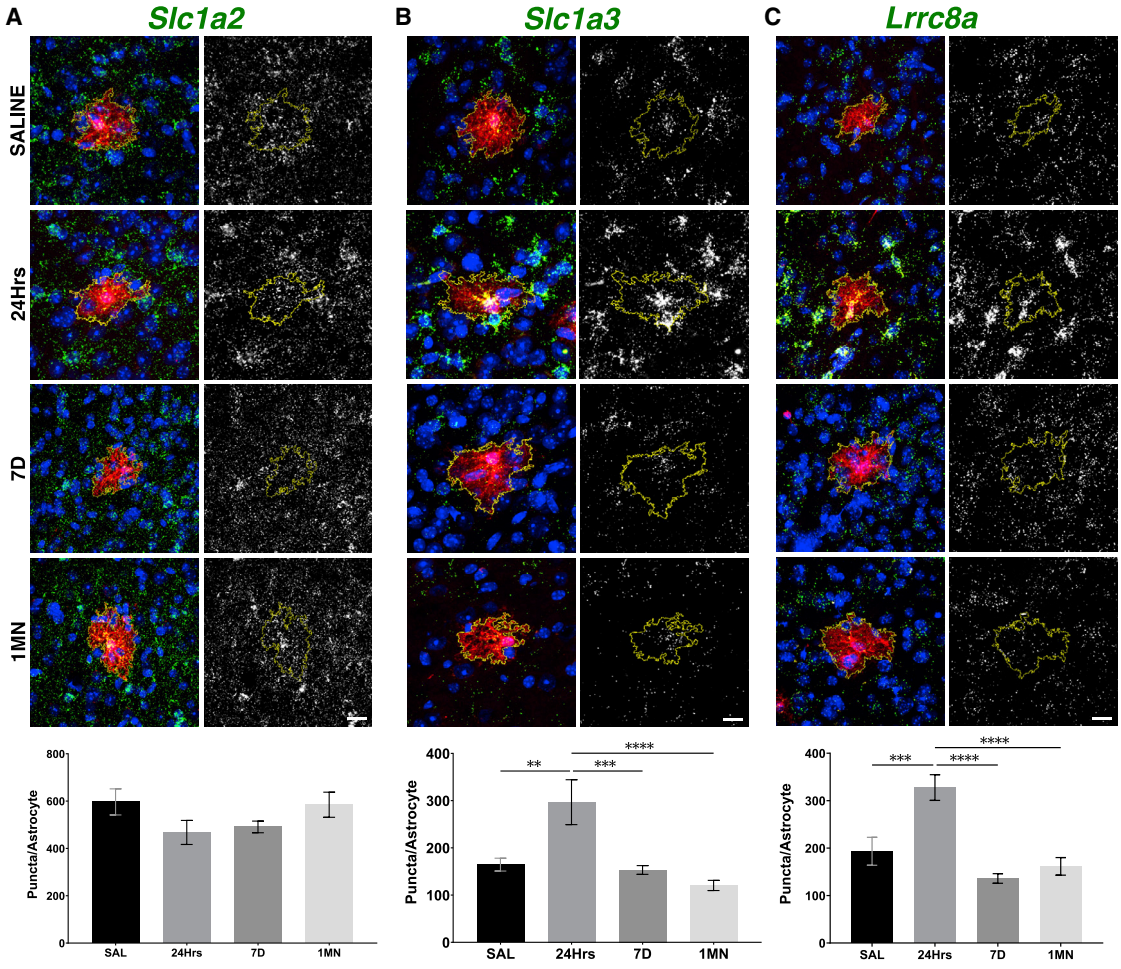

Figure 7. Reactive markers return to baseline levels in astrocytes that were initially reactive

(A–C) RNAScope staining (green) for *Slc1a2* (A), *Slc1a3* (B), and *Lrrc8a* (C) in *Lcn2CreERT2*;*Ai9* animals treated with saline or LPS. Sections were immunostained for tdTomato and counterstained with DAPI. Bottom: quantification of RNAScope puncta per tdTomato$^+$ astrocyte. $^{**}p < 0.01$, $^{***}p < 0.001$, $^{****}p < 0.0001$, ANOVA followed by Tukey's honest significant difference post hoc test. n = 30 pooled astrocytes across three animals. Error bars ± SEM. Scale bars, 20 μm.

specifically. Here we introduce the *Lcn2CreERT2* mouse as a first step to selectively target and manipulate RAs in the diseased or injured brain when used in combination with traditional astrocytic tools.

Advantages and utility of the Lcn2CreERT2 mouse

Lcn2CreERT2 shows no significant basal expression in the CNS, and is strongly upregulated in a number of different disease, infection, and injury models. This is a key aspect of *Lcn2CreERT2*, as existing tools to study RAs have relied on markers such as *GFAP* or *Aldh1l1*, which are already expressed in the healthy CNS (Brambilla et al., 2005; Cahoy et al., 2008; Robel et al., 2009; Sofroniew, 2009; Srinivasan et al., 2016). After most insults there is a mix of reactive and healthy astrocytes (Escartin et al., 2021), so even using tools driven by these promoters for which timing can be controlled (e.g., *CreERT2* lines), both healthy astrocytes and RAs alike will be targeted. Thus, any tool that targets astrocytes before they become reactive has the potential downside of impacting healthy brain function or diluting effects that specifically occur only in RAs. The *Lcn2CreERT2* line takes advantage of the minimal expression of *Lcn2* in the healthy nervous system to ensure that Cre is only expressed after injury and only in reactive cells. This ensures that Cre expression in astrocytes will only be turned on in a reactive setting.

When developing the *Lcn2CreERT2* mouse, a decision was made to use CreERT2, a tamoxifen-dependent Cre recombinase (Figure S1B). A number of floxed transgenic lines and constructs have already been developed that make use of Cre-mediated recombination to activate gene expression, making the *Lcn2CreERT2* mouse highly customizable for study of the immune response and brain disease mechanisms (Birling et al., 2012; Daigle et al., 2018; Van Duyne, 2015). Having the *Lcn2CreERT2* mouse express a Cre-ERT2 allows for temporal control of Cre activation. This approach opens up a number of experimental possibilities. First, Cre activity outside of the preferred experimental window can be prevented. This is an important consideration toward preventing off-target

recombination in other *Lcn2* expressing cells, such as the peripheral immune system. Second, different windows of astrocyte reactivity can be examined during the course of a disease or injury process. For example, in the kainic acid model of epilepsy, after the induction of *status epilepticus* (SE) there is a 1- to 2-week latent period prior to the development of progressive seizures (Coulter and Steinhauser, 2015). By changing the timing of tamoxifen treatment, examination of RAs induced immediately after SE can be compared with those that develop during and after the latent period and leading to chronic stages of the disease. It is very likely that the properties and functions of RAs are very different across time points in disease progression or recovery from injury. By FACS sorting and sequencing RAs at different time points, heterogeneity of RAs *within* a disease process can begin to be appreciated.

As astrocyte reactivity has been observed almost universally in response to CNS injury and disease, one consideration in designing a tool is its ability to be used to study any brain pathology of interest. In the work that initially identified *Lcn2* in RAs (Zamanian et al., 2012), it was suggested to be a pan-RA marker, as its expression was observed in two very different injury models. These models, LPS and stroke, have since been reported to induce at least two broad categories of RAs (Liddelow et al., 2017) that likely represent only two ends of a spectrum, with many subtypes in-between and even within a particular injury or disease process (Anderson et al., 2014). In addition to not being expressed prior to the onset of inflammation, we have thus far found *Lcn2CreERT2* expression in several of the disease models we have explored. *Lcn2CreERT2* is upregulated following IP LPS, *T. gondii* infection, and intrastriatal LPS (Figures 1, 2, and 3), and also in other disease models briefly examined in this paper that will require further investigation (Figure S3). Unsurprisingly, expression of tdTomato in the *5XFAD* mouse was extremely sparse and restricted to thalamus, consistent with a previous mRNA sequencing study that showed that *Lcn2* is not broadly or strongly upregulated in this AD mouse model (Habib et al., 2020). Future studies could continue to expand the number of diseases investigated with the *Lcn2CreERT2* mouse, which would shed light on heterogeneity of RAs.

The ability of the *Lcn2CreERT2* mouse to permanently label RAs with a fluorescent marker opens up a number of experimental possibilities. In our study, we provided proof-of-concept for different directions one could take. First, we were able to isolate labeled Lcn2Cre$^+$ cells using FACS. Isolation of RAs will enable any of several sequencing strategies for the study of gene expression changes in RAs. Second, we were able to explore a long-standing question in the field about the fate of RAs long after acute inflammation (Escartin et al., 2021), a question that has remained unanswered despite recent advances in astrocyte molecular phenotyping (Diaz-Castro et al., 2021; Hasel et al., 2021). By performing longitudinal studies, we observed that the astrocytes that were *Lcn2* positive 1 day after induction of inflammation remained in the CNS long after the inflammatory response subsided. Further, the expression of markers of astrocyte reactivity analyzed in our study returned to basal levels. These findings suggest that astrocytes that become reactive after an acute injury or insult have the capacity to largely revert back their expression profiles to the non-reactive state after the immune and healing response is complete, rather than being tagged for programmed cell death and replaced. What this might mean for the development and progression of brain disease remains to be determined. Future studies could use the *Lcn2CreERT2* mouse to perform longitudinal analysis of the same astrocytes over time using 2-photon microscopy in living mice to address this question further.

Regarding the genes differentially regulated in the tdTomato$^+$ cells of *Lcn2CreERT2*; *Ai9* mice after low-dose LPS treatment compared with saline controls, mining of previous datasets suggest that *Slc1a3/Glast* also trends toward being upregulated in multiple astrocytic populations 24 h after high-dose LPS treatment (Hasel et al., 2021) (https://www.liddelowlab.com/gliaseq; https://gliaseqrev.ue.r.appspot.com). A similar but more striking upregulation was also observed for *Lrrc8a* 24 h after high-dose LPS (Hasel et al., 2021). Consistent with our findings, by 72 h post-LPS treatment the expression of both of these genes appears to revert back to baseline, or at least become noticeably downregulated compared with 24 h. Interestingly, *Lrrc8a* and other *Lrrc8s* are differentially regulated also in the R6/2 model of Huntington disease, but in that case they are downregulated compared with non-carriers (Diaz-Castro et al., 2019). The exploration of the role of VRAC/Lrrc8 in the etiology and progression of a variety of brain disorders is an area of active interest (Mongin, 2016; Yang et al., 2019).

The observation that activated cells are likely to remain in the CNS raises a number of interesting questions for further study. RAs undergo a number of changes that may impact their normal homeostatic functions (Sofroniew, 2015). It is currently unknown if an RA that can revert back to a non-reactive state is able to perform its key homeostatic functions as efficiently as before the injury. Our data showed that one morphological feature of reactivity, increased complexity of distal processes, fails to revert back to baseline levels even 30 days after inflammation, suggesting that some effects of the inflammatory process might be long lasting. Given the emerging relationship between astrocyte morphology and function (Lawal et al., 2022) in the future it will be interesting to investigate how this long-lasting effect on number of distal branches affects astrocyte physiology. In this regard, the *Lcn2CreERT2* mouse will be useful to analyze many key functions of astrocytes before, during, and after injury (or in disease progression), such as glutamate uptake and potassium buffering, synaptogenesis and synaptic maintenance, regulation of the brain extracellular space, and cerebrovascular coupling, to name a few. Fluorescent labeling also opens the possibility to examine RAs in real time in living mice across disease and injury progression, allowing a live look-in at some of the more controversial aspects of reactivity, such as migration, proliferation, and changes in astrocyte connectivity (Escartin et al., 2021).

Limitations of the study

The *Lcn2CreERT2* mouse has three main limitations when it comes to the study of RAs. Although Cre was expressed in RAs in a number of different disease models, the percentage of *Lcn2CreERT2* expressing astrocytes was far lower than the percentage of cells stained for GFAP or endogenous *Lcn2*. This limitation is compounded by the fact that *Lcn2*, which was

initially thought to be upregulated in most mouse brain disease models, does not appear to be strongly upregulated in models of Alzheimer or Huntington disease (Diaz-Castro et al., 2019; Habib et al., 2020; Zamanian et al., 2012). In addition, there seems to be some regional specify to the expression of *Lcn2CreERT2* in astrocytes. While most areas of the forebrain expressed TdTomato in *Lcn2CreERT2*;*Ai9* animals after induction of inflammation, labeling of astrocytes was widespread in thalamus and hypothalamus, somewhat limited in the dorsal cortex, and very low in the dorsal hippocampus (Figure S2E). While there might be many reasons behind the specificity in *Lcn2CreERT2* expression, from alternative splicing of the targeted exon to existence of alternative *Lcn2* promoters, the expression pattern could be revealing underlying regional biological differences in RAs. Molecular, functional, and morphological differences have been noted for several other regions in the healthy and diseased brain, and this might just be one more example of astrocyte heterogeneity (Adams and Gallo, 2018; Anderson et al., 2014; Sofroniew, 2015).

The third potential limitation is expression of *Lcn2CreERT2* in non-astrocytic cells. *Lcn2CreERT2* is also expressed in endothelial cells following LPS, which was expected from our initial observations of endogenous *Lcn2* expression. Therefore, *Lcn2CreERT2* could also be a useful tool for the study of reactive endothelial cells and the BBB in brain injury and disease. In order to focus our study on RAs specifically, we used a combinatorial approach in which an AAV viral construct AAV-*GFAP(long)-FLEX-GCaMP7f* was used to drive expression of Cre-dependent GCaMP7 under the GFAP promoter. The use of this approach allowed us to intersect targeting of reactive cells (*Lcn2CreERT2*) with astrocytes (GFAP), thereby preventing LPS-induced endothelial expression of Cre. As we were able to observe robust expression of GCaMP7 in astrocytes using this approach, it could be used in future studies to examine changes in RA calcium signaling. Similarly, the use of the *Lcn2CreERT2* line with intersectional transgenic drivers or viral vectors that selectively express GOIs based on the overlapping or sequential expression of multiple recombinases (e.g., Cre and Flp, Cre and Dre) will allow for labeling of subpopulations of reactive cells with greater specificity and also make a variety of Boolean logic operations (AND, NOT, OR) available (Awatramani et al., 2003; Fan et al., 2020; Fenno et al., 2014, 2020; Ubina et al., 2021). For flow cytometry and FACS, combining tdTomato detection with an antibody for a surface marker of astrocytes like ACSA2 could be a suitable solution (Kantzer et al., 2017; Lattke et al., 2021). Overall, we view the *Lcn2CreERT2* mouse as a first generation tool for the study of RAs. As heterogeneity of RAs is explored further, next generation tools could be designed to target other specific subsets of RAs that are predominantly expressed in a particular brain injury or disease process.

STAR★METHODS

Detailed methods are provided in the online version of this paper and include the following:

SUPPLEMENTAL INFORMATION

Supplemental information can be found online at https://doi.org/10.1016/j.crmeth.2022.100276.

ACKNOWLEDGMENTS

The authors thank the Transgenic Mouse Facility (TMF) at the University of California, Irvine, for the generation of the *Lcn2CreERT2* mice. This work was supported by grants from the National Institutes of Health R03AG063264 and R21NS109918 to T.A.F. and M.M.R.; R01DA048815 to E.H.W., T.A.F., and M.M.R.; and R01DA048815-03S1 to E.H.W. The funders had no role in study design, data collection and analysis, decision to publish, or preparation of the manuscript.

AUTHOR CONTRIBUTIONS

W.A-S., T.U., Z.F., E.H.W., T.A.F., and M.M.R. designed the experiments. W.A-S., T.U., Z.F., Y-C.W., E.A.V., and B.R. performed the experiments. W.A-S., T.U., and Z.F. analyzed the data. T.A.F. and M.M.R. conceptualized the study. W.A-S., T.A.F., and M.M.R. wrote the paper. W.A-S., T.U., Z.F., E.H.W., T.A.F., and M.M.R. edited the manuscript.

INCLUSION AND DIVERSITY

One or more of the authors of this paper self-identifies as an underrepresented ethnic minority in science. One or more of the authors of this paper received support from a program designed to increase minority representation in science. While citing references scientifically relevant for this work, we also actively worked to promote gender balance in our reference list.

Received: October 14, 2021
Revised: June 1, 2022
Accepted: July 22, 2022
Published: August 22, 2022

REFERENCES

Adams, K.L., and Gallo, V. (2018). The diversity and disparity of the glial scar. Nat. Neurosci. *21*, 9–15.

Anderson, M.A., Ao, Y., and Sofroniew, M.V. (2014). Heterogeneity of reactive astrocytes. Neurosci. Lett. *565*, 23–29.

Atasoy, D., Aponte, Y., Su, H.H., and Sternson, S.M. (2008). A FLEX switch targets Channelrhodopsin-2 to multiple cell types for imaging and long-range circuit mapping. J. Neurosci. *28*, 7025–7030.

Awatramani, R., Soriano, P., Rodriguez, C., Mai, J.J., and Dymecki, S.M. (2003). Cryptic boundaries in roof plate and choroid plexus identified by intersectional gene activation. Nat. Genet. *35*, 70–75.

Binder, D.K., and Steinhäuser, C. (2006). Functional changes in astroglial cells in epilepsy. Glia *54*, 358–368.

Birling, M.-C., Dierich, A., Jacquot, S., Hérault, Y., and Pavlovic, G. (2012). Highly-efficient, fluorescent, locus directed cre and FlpO deleter mice on a pure C57BL/6N genetic background. Genesis *50*, 482–489.

Brambilla, R., Bracchi-Ricard, V., Hu, W.-H., Frydel, B., Bramwell, A., Karmally, S., Green, E.J., and Bethea, J.R. (2005). Inhibition of astroglial nuclear factor κB reduces inflammation and improves functional recovery after spinal cord injury. J. Exp. Med. *202*, 145–156.

Burda, J.E., and Sofroniew, M.V. (2014). Reactive gliosis and the multicellular response to CNS damage and disease. Neuron *81*, 229–248.

Cahoy, J.D., Emery, B., Kaushal, A., Foo, L.C., Zamanian, J.L., Christopherson, K.S., Xing, Y., Lubischer, J.L., Krieg, P.A., Krupenko, S.A., et al. (2008). A transcriptome database for astrocytes, neurons, and oligodendrocytes: a new resource for understanding brain development and function. J. Neurosci. *28*, 264–278.

Cetin, A., Komai, S., Eliava, M., Seeburg, P.H., and Osten, P. (2006). Stereotaxic gene delivery in the rodent brain. Nat. Protoc. *1*, 3166–3173.

Coulter, D., and Steinhauser, C. (2015). Role of astrocytes in epilpesy. Cold Spring Harb. Perspect. Med. *5*, 1–13.

Daigle, T.L., Madisen, L., Hage, T.A., Valley, M.T., Knoblich, U., Larsen, R.S., Takeno, M.M., Huang, L., Gu, H., Larsen, R., et al. (2018). A suite of transgenic driver and reporter mouse lines with enhanced brain-cell-type targeting and functionality. Cell *174*, 465–480.e22.

Diaz-Castro, B., Gangwani, M.R., Yu, X., Coppola, G., and Khakh, B.S. (2019). Astrocyte molecular signatures in Huntington's disease. Sci. Transl. Med. *11*, 1–13.

Diaz-Castro, B., Bernstein, A.M., Coppola, G., Sofroniew, M.V., and Khakh, B.S. (2021). Molecular and functional properties of cortical astrocytes during peripherally induced neuroinflammation. Cell Rep. *36*, 109508.

Dubey, J.P., Murata, F.H.A., Cerqueira-Cézar, C.K., Kwok, O.C.H., and Villena, I. (2021). Congenital toxoplasmosis in humans: an update of worldwide rate of congenital infections. Parasitology *148*, 1406–1416.

Van Duyne, G.D. (2015). Cre recombinase. In Mobile DNA III, N.L. Craig, M. Chandler, M. Gellert, A.M. Lambowitz, P.A. Rice, and S.B. Sandmeyer, eds. (John Wiley & Sons, Inc.), pp. 119–138.

Eng, L.F., Vanderhaeghen, J.J., Bignami, A., and Gerstl, B. (1971). An acidic protein isolated from fibrous astrocytes. Brain Res. *28*, 351–354.

Engelhardt, B., and Sorokin, L. (2009). The blood–brain and the blood–cerebrospinal fluid barriers: function and dysfunction. Semin. Immunopathol. *31*, 497–511.

Escartin, C., Galea, E., Lakatos, A., O'Callaghan, J.P., Petzold, G.C., Serrano-Pozo, A., Steinhäuser, C., Volterra, A., Carmignoto, G., Agarwal, A., et al. (2021). Reactive astrocyte nomenclature, definitions, and future directions. Nat. Neurosci. *24*, 312–325.

Fan, L.Z., Kheifets, S., Böhm, U.L., Wu, H., Piatkevich, K.D., Xie, M.E., Parot, V., Ha, Y., Evans, K.E., Boyden, E.S., et al. (2020). All-optical electrophysiology reveals the role of lateral inhibition in sensory processing in cortical layer 1. Cell *180*, 521–535.e18.

Fenno, L.E., Mattis, J., Ramakrishnan, C., Hyun, M., Lee, S.Y., He, M., Tucciarone, J., Selimbeyoglu, A., Berndt, A., Grosenick, L., et al. (2014). Targeting cells with single vectors using multiple-feature Boolean logic. Nat. Methods *11*, 763–772.

Fenno, L.E., Ramakrishnan, C., Kim, Y.S., Evans, K.E., Lo, M., Vesuna, S., Inoue, M., Cheung, K.Y.M., Yuen, E., Pichamoorthy, N., et al. (2020). Comprehensive dual- and triple-feature intersectional single-vector delivery of diverse functional payloads to cells of behaving mammals. Neuron *107*, 836–853.e11.

Ferrer-Acosta, Y., Gonzalez-Vega, M.N., Rivera-Aponte, D.E., Martinez-Jimenez, S.M., and Martins, A.H. (2017). Monitoring astrocyte reactivity and proliferation in vitro under ischemic-like conditions. J. Vis. Exp. *2017*, 1–9.

Kantzer, C.G., Boutin, C., Herzig, I.D., Wittwer, C., Reiß, S., Tiveron, M.C., Drewes, J., Rockel, T.D., Ohlig, S., Ninkovic, J., et al. (2017). Anti-ACSA-2 defines a novel monoclonal antibody for prospective isolation of living neonatal and adult astrocytes. Glia *65*, 990–1004.

Habib, N., McCabe, C., Medina, S., Varshavsky, M., Kitsberg, D., Dvir-Szternfeld, R., Green, G., Dionne, D., Nguyen, L., Marshall, J.L., et al. (2020). Disease-associated astrocytes in Alzheimer's disease and aging. Nat. Neurosci. *23*, 701–706.

Hasel, P., Rose, I.V.L., Sadick, J.S., Kim, R.D., and Liddelow, S.A. (2021). Neuroinflammatory astrocyte subtypes in the mouse brain. Nat. Neurosci. *24*, 1475–1487.

Helassa, N., Podor, B., Fine, A., and Török, K. (2016). Design and mechanistic insight into ultrafast calcium indicators for monitoring intracellular calcium dynamics. Sci. Rep. *6*, 38276–38314.

Hunter, R.L., Cheng, B., Choi, D.Y., Liu, M., Liu, S., Cass, W.A., and Bing, G. (2009). Intrastriatal lipopolysaccharide injection induces Parkinsonism in C57/B6 mice. J. Neurosci. Res. *87*, 1913–1921.

Jessen, N.A., Munk, A.S.F., Lundgaard, I., and Nedergaard, M. (2015). The glymphatic system: a beginner's guide. Neurochem. Res. *40*, 2583–2599.

Katsouri, L., Birch, A.M., Renziehausen, A.W.J., Zach, C., Aman, Y., Steeds, H., Bonsu, A., Palmer, E.O.C., Mirzaei, N., Ries, M., and Sastre, M. (2020). Ablation of reactive astrocytes exacerbates disease pathology in a model of Alzheimer's disease. Glia *68*, 1017–1030.

Laird, M.D., Vender, J.R., and Dhandapani, K.M. (2008). Opposing roles for reactive astrocytes following traumatic brain injury. Neurosignals *16*, 154–164.

Lattke, M., Goldstone, R., Ellis, J.K., Boeing, S., Jurado-Arjona, J., Marichal, N., MacRae, J.I., Berninger, B., and Guillemot, F. (2021). Extensive transcriptional and chromatin changes underlie astrocyte maturation in vivo and in culture. Nat. Commun. *12*, 4335.

Lawal, O., Ulloa Severino, F.P., and Eroglu, C. (2022). The role of astrocyte structural plasticity in regulating neural circuit function and behavior. Glia *70*, 1467–1483.

Lee, Y., Messing, A., Su, M., and Brenner, M. (2008). GFAP promoter elements required for region-specific and astrocyte-specific expression. Glia *56*, 481–493.

Liddelow, S.A., Guttenplan, K.A., Clarke, L.E., Bennett, F.C., Bohlen, C.J., Schirmer, L., Bennett, M.L., Münch, A.E., Chung, W.-S., Peterson, T.C., et al. (2017). Neurotoxic reactive astrocytes are induced by activated microglia. Nature *541*, 481–487.

Liu, P., Jenkins, N.A., and Copeland, N.G. (2003). A highly efficient recombineering-based method for generating conditional knockout mutations. Genome Res. *13*, 476–484.

Madisen, L., Zwingman, T.A., Sunkin, S.M., Oh, S.W., Zariwala, H.A., Gu, H., Ng, L.L., Palmiter, R.D., Hawrylycz, M.J., Jones, A.R., et al. (2010). A robust and high-throughput Cre reporting and characterization system for the whole mouse brain. Nat. Neurosci. *13*, 133–140.

Mongin, A.A. (2016). Volume-regulated anion channel–a frenemy within the brain. Pflugers Arch. *468*, 421–441.

Nava Catorce, M., and Gevorkian, G. (2016). LPS-Induced murine neuroinflammation model: main features and suitability for pre-clinical assessment of nutraceuticals. Curr. Neuropharmacol. *14*, 155–164.

Noor, S., Habashy, A.S., Nance, J.P., Clark, R.T., Nemati, K., Carson, M.J., and Wilson, E.H. (2010). CCR7-dependent immunity during acute Toxoplasma gondii infection. Infect. Immun. *78*, 2257–2263.

Okada, S., Nakamura, M., Katoh, H., Miyao, T., Shimazaki, T., Ishii, K., Yamane, J., Yoshimura, A., Iwamoto, Y., Toyama, Y., and Okano, H. (2006). Conditional ablation of Stat3 or Socs3 discloses a dual role for reactive astrocytes after spinal cord injury. Nat. Med. *12*, 829–834.

Panatier, A., and Robitaille, R. (2016). Astrocytic mGluR5 and the tripartite synapse. Neuroscience *323*, 29–34.

Park, J.-S., Kam, T.-I., Lee, S., Park, H., Oh, Y., Kwon, S.-H., Song, J.-J., Kim, D., Kim, H., Jhaldiyal, A., et al. (2021). Blocking microglial activation of reactive

astrocytes is neuroprotective in models of Alzheimer's disease. Acta Neuropathol. Commun. *9*, 78.

Passini, M.A., Watson, D.J., Vite, C.H., Landsburg, D.J., Feigenbaum, A.L., and Wolfe, J.H. (2003). Intraventricular brain injection of adeno-associated virus type 1 (AAV1) in neonatal mice results in complementary patterns of neuronal transduction to AAV2 and total long-term correction of storage lesions in the brains of beta-glucuronidase-deficient mi. J. Virol. *77*, 7034–7040.

Peterson, A.R., and Binder, D.K. (2019). Post-translational regulation of GLT-1 in neurological diseases and its potential as an effective therapeutic target. Front. Mol. Neurosci. *12*. https://doi.org/10.3389/fnmol.2019.00164.

Robel, S., Mori, T., Zoubaa, S., Schlegel, J., Sirko, S., Faissner, A., Goebbels, S., Dimou, L., and Götz, M. (2009). Conditional deletion of β1-integrin in astroglia causes partial reactive gliosis. Glia *57*, 1630–1647.

Salic, A., and Mitchison, T.J. (2008). A chemical method for fast and sensitive detection of DNA synthesis in vivo. Proc. Natl. Acad. Sci. USA *105*, 2415–2420.

Schindelin, J., Arganda-Carreras, I., Frise, E., Kaynig, V., Longair, M., Pietzsch, T., Preibisch, S., Rueden, C., Saalfeld, S., Schmid, B., et al. (2012). Fiji: an open-source platform for biological-image analysis. Nat. Methods *9*, 676–682.

Shinozaki, Y., Shibata, K., Yoshida, K., Shigetomi, E., Gachet, C., Ikenaka, K., Tanaka, K.F., and Koizumi, S. (2017). Transformation of astrocytes to a neuroprotective phenotype by microglia via P2Y1Receptor downregulation. Cell Rep. *19*, 1151–1164.

Schnütgen, F., Doerflinger, N., Calléja, C., Wendling, O., Chambon, P., and Ghyselinck, N.B. (2003). A directional strategy for monitoring Cre-mediated recombination at the cellular level in the mouse. Nat. Biotechnol. *21*, 562–565.

Sofroniew, M. v (2009). Molecular dissection of reactive astrogliosis and glial scar formation. Trends Neurosci. *32*, 638–647.

Sofroniew, M.V. (2015). Astrogliosis. Cold Spring Harb. Perspect. Biol. *7*. a020420-16.

Sofroniew, M. v (2020). Astrocyte reactivity : subtypes , states , and functions in CNS innate immunity. Trends Immunol. *41*, 758–770.

Sofroniew, M.V., and Vinters, H.V. (2010). Astrocytes: Biology and pathology. Acta Neuropathol. *119*, 7–35.

Srinivasan, R., Lu, T.-Y., Chai, H., Xu, J., Huang, B.S., Golshani, P., Coppola, G., and Khakh, B.S. (2016). New transgenic mouse lines for selectively targeting astrocytes and studying calcium signals in astrocyte processes in situ and in vivo. Neuron *92*, 1181–1195.

Stoica, L., Ahmed, S.S., Gao, G., and Sena-Esteves, M. (2013). Gene transfer to the CNS using recombinant adeno-associated virus. Curr. Protoc. Microbiol. https://doi.org/10.1002/9780471729259.mc14d05s29.

Ubina, T., Vahedi-Hunter, T., Agnew-Svoboda, W., Wong, W., Gupta, A., Santhakumar, V., and Riccomagno, M.M. (2021). ExBoX – a simple Boolean exclusion strategy to drive expression in neurons. J. Cell Sci. *134*, jcs257212.

Ung, K., Tepe, B., Pekarek, B., Arenkiel, B.R., and Deneen, B. (2020). Parallel astrocyte calcium signaling modulates olfactory bulb responses. J. Neurosci. Res. *98*, 1605–1618.

Wallberg, F., Tenev, T., and Meier, P. (2016). Analysis of apoptosis and necroptosis by fluorescence-activated cell sorting. Cold Spring Harb. Protoc. *2016*, pdb.prot087387. https://doi.org/10.1101/pdb.prot087387.

Wanner, I.B., Anderson, M.A., Song, B., Levine, J., Fernandez, A., Gray-Thompson, Z., Ao, Y., and Sofroniew, M.V. (2013). Glial scar borders are formed by newly proliferated, elongated astrocytes that interact to corral inflammatory and fibrotic cells via STAT3-dependent mechanisms after spinal cord injury. J. Neurosci. *33*, 12870–12886.

Wheeler, M.A., Clark, I.C., Tjon, E.C., Li, Z., Zandee, S.E.J., Couturier, C.P., Watson, B.R., Scalisi, G., Alkwai, S., Rothhammer, V., et al. (2020). MAFG-driven astrocytes promote CNS inflammation. Nature *578*, 593–599.

Wilhelmsson, U., Bushong, E.A., Price, D.L., Smarr, B.L., Phung, V., Terada, M., Ellisman, M.H., and Pekny, M. (2006). Redefining the concept of reactive astrocytes as cells that remain within their unique domains upon reaction to injury. Proc. Natl. Acad. Sci. USA *103*, 17513–17518.

Wohlfert, E.A., Blader, I.J., and Wilson, E.H. (2017). Brains and brawn: Toxoplasma infections of the central nervous system and skeletal muscle. Trends Parasitol. *33*, 519–531.

Yang, J., Vitery, M.D.C., Chen, J., Osei-Owusu, J., Chu, J., and Qiu, Z. (2019). Glutamate-releasing SWELL1 channel in astrocytes modulates synaptic transmission and promotes brain damage in stroke. Neuron *102*, 813–827.e6.

Yun, S.P., Kam, T.I., Panicker, N., Kim, S., Oh, Y., Park, J.S., Kwon, S.H., Park, Y.J., Karuppagounder, S.S., Park, H., et al. (2018). Block of A1 astrocyte conversion by microglia is neuroprotective in models of Parkinson's disease. Nat. Med. *24*, 931–938.

Zamanian, J.L., Xu, L., Foo, L.C., Nouri, N., Zhou, L., Giffard, R.G., and Barres, B.A. (2012). Genomic analysis of reactive astrogliosis. J. Neurosci. *32*, 6391–6410.

STAR★METHODS

KEY RESOURCES TABLE

REAGENT or RESOURCE	SOURCE	IDENTIFIER
Antibodies		
Rabbit polyclonal anti-DSRed	Takara Bio	Cat#632496; RRID: AB_10013483
Rat monoclonal anti-GFAP	Invitrogen	Cat#13-0300; RRID: AB_86543
Chicken polyclonal anti-Foxo3	EnCor	Cat#CPCA-FOX3; RRID: AB_2747400
Chicken polyclonal anti-GFP	AVES	Cat#GFP-1020; RRID: AB_10000240
Bacterial and virus strains		
AAV-GFAP(long)-FLEX-GCAMP7f	This paper/Vector builder	Addgene ID: 189612
Biological samples		
Me49 strain of *Toxoplasma gondii*	This paper	N/A
Chemicals, peptides, and recombinant proteins		
Lipopolysaccharides from *Escherichia coli*	Sigma-Aldrich	L2880
Tamoxifen	Sigma-Aldrich	T5648
5-ethynul-2′-deoxyuridine (EdU)	Molecular Probes	E10187
Tomato-lectin	Vector Laboratories	B-1175
Opal 520	Akoya Biosciences	FP1487001KT
Opal 690	Akoya Biosciences	FP1497001KT
Critical commercial assays		
RNAScope Multiplex Fluorescent Detection kit v2	Advanced Cell Diagnostics	323110
Click-iT EdU Cell Proliferation Kit	Invitrogen	C10337
Experimental models: Organisms/strains		
Mouse: *Lcn2CreERT2*	This paper	N/A
Mouse: Swiss Webster	Taconic	SW-F, SW-M
Mouse: B6.Cg-Gt(ROSA)26Sortm9(CAG-tdTomato)Hze/J (Ai9)	The Jackson Laboratory	Cat#007909; RRID: IMSR_JAX:007909
Oligonucleotides		
Slc1a3 probe	Advanced Cell Diagnostics	430781
Lcn2 probe	Advanced Cell Diagnostics	313971
Pecam1 probe	Advanced Cell Diagnostics	316721
Lrrc8a probe	Advanced Cell Diagnostics	458371
Slc1a2 probe	Advanced Cell Diagnostics	441341
Aldh1l1 probe	Advanced Cell Diagnostics	405891
Gfap probe	Advanced Cell Diagnostics	313211
Primer: *Lcn2CreERT2* forward: 5′-GGCAGTCCAGATCTGAGCTGC-3′	This paper	N/A
Primer: *Lcn2CreERT2* reverse: 5′-TGCATCGACCGGTAATGCAGG-3′	This paper	N/A

RESOURCE AVAILABILITY

Lead contact

Further information and requests for resources and reagents should be directed to and will be fulfilled by the lead contact, Martin M. Riccomagno (martinmr@ucr.edu).

Materials availability

The *Lcn2CreERT2* mouse line is available upon request from the lead contact. The GFAP-FLEX-GCAMP7f plasmid has been deposited at Addgene (ID: 189612)

Data and code availability

- All data reported in this paper will be shared by the lead contact upon request.

- This paper does not report original code.
- Any additional information required to reanalyze the data reported in this paper is available from the lead contact upon request.

EXPERIMENTAL MODEL AND SUBJECT DETAILS

Animals

Wild-type Swiss Webster mice were used for histology to examine LCN-2 expression in the naive and inflamed brain. *Lcn2CreERT2* animals were maintained in the Swiss Webster background and crossed into the *Ai9* tdTomato reporter line (strain #007909) available from JAX for experiments. Cre-negative controls were *Lcn2CreERT2* negative littermates, while saline controls were performed on Cre positive littermates. All procedures were done on animals 4-6 months of age. For each experiment at least one male and 1 female were included. Mice were maintained in a 12-hour light/dark cycle with *ad libitum* food and water at room temperature. All animal procedures detailed in the following sections were preformed according to the University of California, Riverside's Institutional Animal Care and Use Committee (IACUC) guidelines.

T. gondii

The Me49 Toxoplasma strain was maintained *in vivo* by passaging consecutively in Swiss Webster (SW) and CBA mice (JAX).

Mouse distribution

The *Lcn2CreERT2* mouse line is available upon request from the lead contact.

METHOD DETAILS

Generation of Lcn2CreERT2 mice

The mouse line carrying a CreERT2 between the *Lcn2* promoter and the 5′ untranslated region (UTR) of the *Lcn2* gene was generated using the vector pBS-PGK-DTA-pa, modified by Bac recombineering (Liu et al., 2003). The *Lcn2-CreERT2*^{neo} allele was engineered to encode for an ERT2 tagged Cre recombinase upstream of the 5′ UTR and an FTR-flanked *neomycin* cassette. Targeting and selection of Embryonic Stem (ES) cells, and production of chimeric mice by injection of targeted ES cells into blastocysts was performed by the Transgenic Mouse Facility (TMF) at the University of California, Irvine. Germline transmission of the *Lcn2-CreERT2*^{neo} allele was verified by southern blot and a PCR genotyping strategy. In order to eliminate the *neomycin* cassette, *Lcn2-CreERT2*$^{neo/+}$ animals were crossed to the deleter mice carrying ACT-FlpE, which expresses FlpE recombinase under the ACTB promoter. Expression of FlpE generates the *Lcn2CreERT2* allele by removal of the *neomycin* gene while leaving a single FRT site in the genomic DNA. All breeding at the chimera stage was conducted in C57/B16J mice and subsequently outbred to the Swiss Webster background for at least 3 generations. PCR genotyping of the *Lcn2CreERT2* mouse was conducted using the following primers: *Lcn2CreERT2* Forward: 5′-GGCAGTCCAGATCTGAGCTGC-3′ and *Lcn2CreERT2* Reverse: 5′-TGCATCGACCGGTAATGCAGG-3′.

Treatments and surgeries

Low-dose and high-dose LPS treatments

Lcn2CreERT2 animals crossed into the *Ai9* tdTomato reporter line were separated into 4 treatment groups; Oil and Saline, Oil and LPS, tamoxifen and saline, and tamoxifen and LPS. Animals in the two tamoxifen treated groups were given an oral gavage of 150 μg/g of tamoxifen (Sigma Aldrich, T5648) dissolved in corn oil (Sigma Aldrich, C8267), while animals in the two oil groups received an equivalent dose of corn oil. Tamoxifen/oil treatments were given every 24 hours for 6 consecutive days. Twenty-four hours after the first tamoxifen or oil treatment, animals in the two LPS treatment groups received intraperitoneal (IP) injections of 1.5 mg/kg lipopolysaccharide (Sigma Aldrich; L2880, Lots 68M4053v and 39M4004v) dissolved in sterile 1x phosphate buffered saline (PBS), while animals in the two saline treated groups received an equivalent dose of sterile 1x PBS. LPS/saline treatments occurred every 24 hours for 5 consecutive days. Animals were collected for tissue processing 24 hours to 1 month following the final treatment.

For experiments utilizing 5-ethynyl-2′-deoxyuridine (EdU), *Lcn2-CreERT2;Ai9* mice were treated with the low dose LPS protocol described above and given 150 mg/kg of EdU (Molecular Probes, cat#E10187) IP on days 4 and 5 of LPS treatment and the following day (3 total doses). Animals collected at the 24-hour post LPS timepoint were given EdU 2 hours prior to collection. Animals were also collected 7 days or 1 month following LPS treatment.

The same treatment groups as described for the low-dose experiment were used for the high-dose LPS treatments. However, for these experiments Tamoxifen/oil treatments were given every 24 hours for only 3 consecutive days. Twenty-four hours after the first tamoxifen or oil treatment, animals in the LPS treatment groups received a single IP injection of 10 mg/kg lipopolysaccharide dissolved in sterile 1x PBS, while animals in the saline treated groups received an equivalent dose of sterile 1x PBS. Animals were collected for tissue processing 24 hours to 1 month following the final treatment.

Toxoplasma gondii injections

To induce chronic Toxoplasma infection, mice were infected viaIP with the cyst forming Me49 Toxoplasma strain maintained *in vivo* by passaging consecutively in Swiss Webster (SW) and CBA mice (JAX). Brains from CBA mice were harvested,

homogenized in 3ml sterile 1X Phosphate Buffer Saline (PBS) through needle passing, and cysts counted using a 30ul aliquot and a light microscope (average cyst burden/brain ~3000). Cyst homogenate was then diluted in sterile 1X PBS and 10 Me49 cysts injected via 200 ul i.p. injections. This amount mimics a physiological Toxoplasma infection that initiates in the gut of the host and travels through the blood stream to eventually enter the brain to form cysts in neurons. Mice were monitored closely immediately after infection to watch for any adverse effects. Following at least three weeks post infection, experimental animals, Lcn2CreERT2; Ai9 tdTomato mice were infected with 10 Me49 *T.gondii* cysts diluted in 1X PBS via 200ul i.p. injections. Three weeks following the initial infection date, when acute systemic inflammation has subsided and infection is localized to the brain, Lcn2CreERT2; Ai9 tdTomato mice were given 150 ug/g tamoxifen dissolved in corn oil. Tamoxifen treatments continued 3 times per week for 4 weeks. Twenty-four hours after the final tamoxifen treatment, animals were collected for tissue processing.

Intrastriatal LPS

Lcn2CreERT2 animals crossed into the *Ai9* tdTomato reporter line were given 150 ug/g tamoxifen dissolved in corn oil every 24 hours for 3 consecutive days. Striatal LPS was injected as described in Hunter et al. (2009). Briefly, on the day of the second tamoxifen treatment animals were stereotactically injected with 1 μl of sterile saline or 1μl of 7.5 mg/ml LPS in four locations in the striatum using the following coordinates from Bregma: a/p +1.18 mm, m/l ± 1.5 mm, and d/v −3.5 mm as well as a/p −0.34 mm, m/l ± 2.5 mm, and d/v −3.2 mm. Injections were performed at 0.5 μl/minute and the needle was kept in place for 5 minutes prior to withdrawing. Animals were kept on a heating pad and received sterile saline subcutaneously until they became hydrated and free moving. Seven days after the injections, animals were collected for tissue processing.

Generation of the AAV-GFAP (long)-FLEX-GCAMP7f vector and stereotactic injections

The AAV-*GFAP(long)-FLEX-GCAMP7f* construct was designed in house. Briefly, a FLEX/DIO cassette (Atasoy et al., 2008; Schnütgen et al., 2003) for *GCaMP7f* in an inverted orientation with respect to a promoter was placed downstream of the *GFAP2.2* promoter (Lee et al., 2008) in an AAV backbone (Figure S4C). The actual vector was then generated and packaged into AAV(PHP.eB) by Vector Builder (Lot 200314AAVW07; $2.53x10^{13}$ GC/ml). Stereotactic injections were performed as previously described on *Lcn2CreERT2* animals. Mice were put under isoflurane anesthesia for the duration of the procedure. Injections of AAV(PHP.eB)-GFAP(long)-FLEX-GCAMP7f (1×10^{13} GC/ml) were performed targeting the right thalamus (coordinates: a/p -1.70 mm, m/l -1.00 mm, d/v -3.00 mm). Mice were injected with 250 nl using a Hamilton Neuros 32 gauge syringe at 75 nl/min. Three weeks after AAV injection, mice were gavaged with tamoxifen for 3 consecutive days, and given 10 mg/kg LPS or equivalent saline on the second day of tamoxifen. Three days after the final tamoxifen treatment, brains were collected and stained for GFP to amplify the GCaMP7 signal.

Flow cytometry

To isolate astrocytes, mouse brains were perfused with sterile 1x PBS and placed in RPMI media (Gibco, 11875101) containing 1% FCS (Corning, MT35015CV) and 25mN HEPES. Perfused brains were transferred to a chilled 60 mm petri dish, passed through an 18g syringe needle, and treated with 4 ml of 0.25% trypsin. Brain suspension was digested at 37°C for 30 minutes in 50 ml conical tubes. During digestion, the mixture was inverted every 5 minutes. Trypsin digestion was stopped with the addition of 30 ml RPMI containing 20% FCS and centrifuged at 1000 rpm for 5 minutes at 4°C. Supernatant was decanted and the pellet resuspended in RPMI (1% FCS) to a total volume of 7 ml. The suspension was transferred to a conical tube with 3 ml of 100% Percoll (Sigma Aldrich, P1644), gently mixed and underlaid with1 ml of 70% Percoll. Samples were centrifuged at 2500 RPM for 20 minutes at 4°C. Following density separation, glial cells were harvested from the interphase and washed in RPMI (1% FCS) and resuspended in FACS buffer for cell sorting. DAPI was added to the FACS buffer to identify dead cells (Wallberg et al., 2016). The samples were analyzed using the MoFLo Astrios EQ Cell Sorter and data were analyzed using FlowJo 10.1.

Fluorescent *in situ* hybridization: RNAScope

Fluorescent *in situ* hybridization was performed on mouse tissue using the RNAScope Multiplex Fluorescent Detection kit v2 (Advanced Cell Diagnostics, ACD, 323110). In this assay, the target RNAs are hybridized to single stranded DNA "z-probes" composed of a complementary ~20 nucleotide sequence to the RNA of interest, a spacer sequence, and a 14 nucleotide tail region. Twenty-eight nucleotide -reamplifier oligos bind to the tail region of z-probe pairs bound to adjacent sequences in the RNA, which are then bound to amplifiers that are labeled with horseradish peroxidase (HRP) enzyme molecules. Tyramide-conjugated fluorophores are added, leading to HRP enzymatic conversion of tyramide into a highly oxidized intermediate which covalently binds to proteins near the HRP label, thus depositing a large number of detectable fluorophores. Multiple RNA targets can be labeled with the use of detection probes in different channels with distinct tail sequences which allow for the generation of unique amplification trees for each target. Each target/probe is then sequentially developed using tyramide signal amplification by using channel specific HRP labels and tyramide conjugated dyes Opal 520 and Opal 690 (Akoya Biosciences, FP1487001KT and FP1497001KT). Probes used were: *Slc1a3* (ACD, 430781), *Lcn2* (ACD, 313971), *Pecam1* (ACD, 316721), *Lrrc8a* (ACD, 458371), *Slc1a2* (ACD, 441341), *Aldh1l1* (ACD, 405891) and *Gfap* (ACD, 313211). At the end of signal development, sections were counterstained with DAPI (Thermo Scientific, 62248) or selected for immunohistochemistry as described below.

Immunofluorescence

Mice were perfused and extracted brains were fixed with 4% paraformaldehyde for 2 hours to overnight at 4°C, rinsed, and sunk in 30% sucrose overnight prior to being frozen in Optimum Cutting Temperature media (OCT, Tissue-Tek, 4583) for cryopreservation. Coronal sections (20 μm) were obtained on a Leica CM3050 cryostat. Sections that were immediately used for immunohistochemistry were next blocked in 10% goat serum and 0.1% Triton-X100 (Thermo Fisher, A16046.AP) for 1 hr at room temperature. This step was skipped for sections that had been previously used for RNAscope, but all steps following were the same. Sections were then incubated overnight at 4°C with primary antibodies. Following incubation, sections were washed with PBS and incubated with secondary antibodies and DAPI. Sections were washed in PBS and mounted using Vectorshield hard-set fluorescence mounting medium (Vector Laboratories, H-1400-10). Confocal fluorescence images were taken using a Leica SPE II microscope. Primary antibodies used in this study include rabbit anti-DSRed (Takara Bio, 632496, 1:500), rat anti-GFAP (Invitrogen, 13-0300, 1:1000), chicken anti-Foxo3 (EnCor CPCA-FOX3, 1:1000), and chicken anti-GFP (AVES, GFP-1020, 1:1000). Tomato-lectin (Vector Laboratories, B-1175-1, 1:75) was combined with primary antibodies. Secondary antibodies used in this study include goat anti-rabbit 488 (Invitrogen, A-11034), goat anti-rat 488 (Invitrogen, A-11006), goat anti-rat 647 (Invitrogen, A-21247), goat anti-chicken 488 (Invitrogen, A11039), streptavidin 488 (Invitrogen, S32354). For EdU experiments, the Click-iT EdU Cell Proliferation Kit from Invitrogen was used according to manufacturer instructions (cat# C10337).

QUANTIFICATION AND STATISTICAL ANALYSIS

Image analysis

All images were analyzed using FIJI (Schindelin et al., 2012). Cells expressing tdTomato were counted by thresholding to create a binary image, the "watershed" function was used and followed by the "analyze particles function" to count cells with a size between 20-2000 pixels^2. Colocalization of IHC markers was performed by manual counting. Cells expressing tdTomato were identified and their area was turned into outlines. For EdU experiments the number of EdU and tdTomato copositive cells was taken as a percentage of total tdTomato labeled cells. Cells showing expression of markers labeled in the green or far-red channel within the outlined areas were then manually counted.

Astrocytes were traced using Neurolucida 360 version 2021.1.3 (MBF Bioscience, Williston, VT USA) and analyzed as previously described (Wilhelmsson et al., 2006). Briefly, the number of cellular processes leaving the soma were counted as well as the number of processes at 15 μm away from the soma. Volume was measured by taking 0.2 μm optical sections and calculating volume from the tdTomato labeling of astrocytes.

Total expression of RNAs identified through FISH was performed by analyzing total fluorescent area in selected ROIs. ROIs were drawn around the thalamus. Background fluorescence was subtracted with the "subtract background" function. The "measure" function was then used to look at total fluorescent area in the drawn ROI. For measuring expression of reactive markers within tdTomato positive astrocytes, the tdTomato positive cells were outlined and the outline was turned into an ROI. The fluorescent channel corresponding to the RNA was then made binary, the watershed function applied, and particles were analyzed within the ROI using the "analyze particles" function. All counts are reported with ± standard error of the mean.

Statistical analysis

Statistical analyses were performed using GraphPad Prism version 9.3.1 for Windows, GraphPad Software, San Diego, California USA, www.graphpad.com. Each figure panel and legend contains information on statistical tests performed along with sample sizes and p values. *$p < 0.05$; **$p < 0.01$; ***$p < 0.001$; ****$p < 0.0001$ for all statistical analyses presented in figures. Sample sizes are mentioned in figure legends.